Astron. Astrophys. 353, 440–446 (2000)

ASTRONOMY AND ASTROPHYSICS

The X-ray background and the evolution of AGN

F. Pompilio, F. La Franca, and G. Matt

Dipartimento di Fisica, Università degli Studi "Roma Tre", Via della Vasca Navale 84, 00146 Roma, Italy

Received 30 July 1999 / Accepted 8 October 1999

Abstract. We discuss the constraints on the AGN evolution from the cosmic X–ray background and source counts. A synthesis model to fit the X–ray background is presented. The data used are a compilation from Gruber (1992), mainly based on HEAO-1 data. The spectrum of type 2 AGN has been modeled including Compton down–scattering within the absorbing material. We found an improvement when a dependence on redshift of the relative number of obscured sources is introduced. In particular, we found a decrease of the fraction of type 2 AGN at redshifts larger than $\sim$2.

However, only the soft X–ray counts are well reproduced, while the hard (5–10 keV) BeppoSAX/HELLAS source counts are underestimated by a factor of $\sim$1.5. A satisfactory global solution, including the good reproduction of the hard counts, is instead obtained if the XRB normalization, recently obtained from BeppoSAX/MECS measurements (about 30% higher than HEAO-1), is adopted.

Key words: cosmology: diffuse radiation – X-rays: general – galaxies: nuclei – galaxies: luminosity function, mass function

1. Introduction

The cosmic X–ray background (XRB) above ~ 1 keV is known to be produced by integrated emission of discrete sources. XRB synthesis models are usually based on the so-called unification scheme for Active Galactic Nuclei (AGN), which ascribes the different observational appearances to the orientation of a molecular torus surrounding the nucleus. The intersection of the line of sight with the torus determines a type 2 AGN (AGN2), while the direct observation of the nucleus identifies a type 1 AGN (AGN1) (Antonucci & Miller 1985). An appropriate combination of the two type of sources can reproduce the main characteristics of high-energy XRB, i.e. intensity and spectral shape (Setti & Woltjer 1989; Madau et al. 1994; Matt & Fabian 1994; Celotti et al. 1995; Comastri et al. 1995).

In this paper, the constraints on the evolution of AGN from the XRB and the source counts are examined, and a possible variation of the standard model (Comastri et al. 1995), in which the AGN2/AGN1 ratio changes with redshift, is explored. We made use of source counts data in the 0.5–2 keV band by ROSAT (Georgantopoulos et al. 1996), in the 0.3–3.5 keV band by *Einstein* (EMSS; Gioia et al. 1990), and the source counts provided by the BeppoSAX HELLAS survey in the 5–10 keV band (Fiore et al. 1999; Comastri et al. 1999). The XRB fitting procedure was based on the Gruber (1992) compilation of data, mostly from HEAO-1 in the 3–50 keV range (Marshall et al. 1980).

Throughout this paper, a Hubble constant $H_0 = 50$ Km s^{-1} Mpc^{-1} and deceleration parameter $q_0 = 0.5$ have been assumed.

Send offprint requests to: F. Pompilio
(pompilio@abell.fis.uniroma3.it)

2. Models for X-ray spectra and evolution of AGN

2.1. AGN1 and AGN2 spectra

The local AGN spectrum is assumed to be the sum of AGN1 and AGN2 spectra ($F_1(E)$, $F_2(E)$ respectively) weighted by the number ratio of AGN2 to AGN1, R:

$$F_{loc}(E) \propto [F_1(E) + R \times F_2(E)] \,.$$

Following Comastri et al. (1995), a double power-law with a Compton reflection component $F_r(E)$ has been adopted for the AGN1 spectrum:

$$F_1(E) \propto \begin{cases} E^{-\alpha_1} & E < 1.5\ keV \\ E^{-\alpha_2} e^{-\frac{E}{E_c}} + F_r(E) & E > 1.5\ keV \end{cases}$$

with α_2=0.9 (Matsuoka et al. 1990; Pounds et al. 1990; Nandra & Pounds 1994), and α_1=1.3.

The steeper, low-energy ($E < 1.5$ keV) spectrum represents the so-called soft excess. The shape and contribution of this component is not well known, and in many sources evidence for its very existence is lacking altogether. As a baseline, we have adopted the same prescription as Comastri et al. (1995), but as it now appears to be rather extreme, we have also explored the opposite case, i.e. no soft excess at all (see Sect. 3.1).

The adopted value of the cut-off energy E_c=400 keV is also similar to those used in previous models (Comastri et al. 1995; Celotti et al. 1995) even if recent BeppoSAX results (Matt et al. 1999a and references therein) seem to suggest somewhat smaller values, but with a rather large spread. The number of sources with reliably measured values is so low, however, that

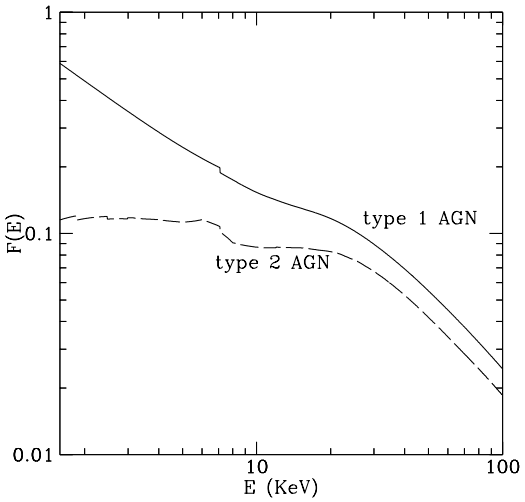

Fig. 1. The AGN1 spectrum (solid line) and the AGN2 average spectrum (dashed line) as produced by the model.

we preferred to still use the values adopted in previous models, to make easier the comparison. In any case, we tested the effect of adopting lower values for the cut–off, and found that the peak in the XRB spectrum at $\sim$ 30–40 keV is less well fitted.

The term $F_r(E)$ represents the Compton reflection component by the accretion disk and by the torus inner surface and has been evaluated following Magdziarz & Zdziarski (1995), assuming an inclination angle of 60°.

According to unified schemes, AGN2 spectra are obtained as AGN1 spectra seen through absorbing matter. The distribution of equivalent hydrogen column density (N_H) is chosen to be logarithmic, i.e. $\frac{dN(log\ N_H)}{d(log\ N_H)} \propto log\ N_H$, that is a reasonable analytical approximation to the recent data on Seyfert galaxies (Maiolino et al. 1998; Risaliti et al. 1999).

As described in a previous paper (Matt et al. 1999b), we developed a transmitted spectrum model by means of Monte Carlo simulations, assuming a spherical geometry with the X-ray source in the centre and considering photoelectric absorption, Compton scattering and fluorescence (for iron atoms only), fixing element abundances as tabulated in Morrison & McCammon (1983).

This transmitted component, which is relevant for $N_H \geq 10^{23} cm^{-2}$, has been so far included in XRB synthesis models only by a handful of authors (Madau et al. 1994; Celotti et al. 1995; Matt et al. 1999b; Wilman & Fabian 1999). The final spectrum $F_{N_H}(E)$ has been then averaged over the N_H-distribution to obtain the total AGN2 spectrum:

$$F_2(E) = \frac{\int_{log\ N_{H1}}^{log\ N_{H2}} F_{N_H}(E)\ log\ N_H\ d(log\ N_H)}{\int_{log\ N_{H1}}^{log\ N_{H2}} log\ N_H\ d(log\ N_H)}.$$

where the N_H-distribution has been considered in the range $10^{21} \leq N_H \leq 10^{25} cm^{-2}$.

The AGN1 and AGN2 spectra are shown in Fig. 1. The AGN1 spectrum is flattened by the reflection component, whose contribution reaches $\sim$ 1/3 of the total at its maximum ($E \sim$ 30 keV). The addition of a transmitted component significantly affects the total AGN2 spectrum, again with a flattening around 30–40 keV. The Compton scattered photons in AGN2 increases the total spectrum by $\sim$ 20% at $\sim$ 30–40 keV with respect to a model involving only absorption.

The last step in evaluating the overall local spectrum concerns the choice of the number ratio R. Maiolino & Rieke (1995) find $R = 4.0 \pm 0.9$, if type 1.8, 1.9 and type 1.2,1.5 Seyfert galaxies are respectively classified as AGN2 and AGN1: the estimate agrees with previous (Huchra & Burg 1992; Goodrich et al. 1994) and more recent (Ho et al. 1997) results, and so $R = 4.0$ has been adopted.

For the sake of simplicity, iron emission line has not been included, even if it is a common feature in AGN. However, the contribution of the line to the 1.5–7 keV XRB is expected to be less then 7% (Gilli et al. 1999a) and it is smeared out by the integration over the redshift range, so that XRB retains its characteristic smoothness (Schwartz 1992), unless the emission is dominated by a small range of redshifts (Matt & Fabian 1994).

2.2. Cosmological evolution

Hard X-rays ($3 >$ keV) are well suited for the selection of type 1 and, especially, type 2 AGNs as they are less affected by absorption. Until recent past little was known about the evolution of the AGNs in this band. The data obtained from the ASCA satellite have allowed a first determination of the 2–10 keV AGN XLF (Boyle et al. 1997). However the statistics was still poor. On the contrary the AGN1 XLF in the soft X-ray band is retained to be well-known at low and intermediate redshift (Boyle et al. 1994; Page et al. 1996; Jones et al. 1997), while at higher redshift ($z \geq 3$) insufficient sampling and lack of statistics prevent the XLF from being firmly evaluated. Anyhow, X-ray AGN1 are detected up to $z = 4.6$ (Miyaji et al. 1998) and no evidence for a space density turn-over is found up to $z \sim 3$, likewise in the optical (e.g. Kennefick et al. 1996) and radio surveys (Shaver et al. 1999).

For these reasons we chose to tie the AGN evolution to the soft X-ray XLF of AGN1. We used the pure luminosity evolution (PLE) scenario which fits the combined ROSAT and EMSS data on AGN1 space density (Boyle et al. 1994). This corresponds to a local luminosity function that can be represented by a double power-law where the break-luminosity L_*, i.e. the luminosity value corresponding to the slope change, evolves as $L_*(z) \propto (1+z)^k$. In the following, we adopt the PLE H-model of Boyle et al. (1994) (hereafter B94) in the 0.3–3.5 keV band:

$$\Phi(L_{44}) = \begin{cases} \Phi^* L_{44}^{-\gamma_1} & L_{44} < L_* \\ \Phi^* L_*^{(\gamma_2-\gamma_1)} L_{44}^{-\gamma_2} & L_{44} \geq L_* \end{cases}$$

with $\gamma_1 = 1.36$, $\gamma_2 = 3.37$, $L_* = 0.39$, $\Phi^* = 1.45 \times 10^{-6}$ Mpc^{-3} $(10^{44}\,\mathrm{erg\,s^{-1}})^{-1}$ and L_{44}, L_* in unity of $10^{44}\,\mathrm{erg\,s^{-1}}$. The break-luminosity evolution follows:

$$L_*(z) = \begin{cases} L_*(z=0) \times (1+z)^k & z < z_{max} \\ L_*(z=0) \times (1+z_{max})^k & z \geq z_{max} \end{cases}$$

where $k = 2.90$ and $z_{max} = 1.73$. We limited the analysis of AGN1 XLF to a PLE model because the most recent attempts with pure density evolution models, in which the space density $\Phi(L)$ directly evolves in redshift, overproduce the soft XRB (Hasinger 1998). We have also to introduce an AGN2 XLF, which is a matter of strong debate. In the framework of the unification scheme, we assumed the density of AGN2 to be R=4 times that of the corresponding unobscured AGN1. We assumed the N_H-distribution to be independent of the AGN1 source luminosity. A different approach may consist in setting a completely unrelated XLF, but it would involve too many parameters and there are not enough data to yield a reliable estimate.

Boyle et al. (1997) directly measured the AGN1 and AGN2 XLF on a sample of 26 2–10 keV ASCA sources at a flux limit of 5×10^{-14} erg cm^{-2} s^{-1}, combined with the HEAO-1 AGN. The analysis gave a result consistent with the 0.3–3.5 keV AGN1 XLF, albeit the evolution seems to be slower ($k = 2.04$).

3. The XRB synthesis model

The intensity of the XRB has been calculated as follows:

$$I(E) = \int\int \frac{d^2N}{dV\,dL} \frac{F[L, E(1+z)]}{4\pi d_l^2} dL dV$$

where $\frac{d^2N}{dV\,dL}$ is the AGN1 XLF, d_l the luminosity distance, $F[L, E(1+z)]$ the AGN spectrum. Introducing the comoving volume $dV(z)$ and the spectrum normalization K corresponding to the considered luminosity, i.e. $K \int_{\Delta E} F_1(E)dE = L$ (ΔE=0.3–3.5 keV), the above relation can be written as:

$$I(E) = \frac{Kc}{4\pi H_0} \int\int L \frac{d^2N}{dV\,dL} \frac{F_{loc}[E(1+z)]}{(1+z)^2(1+2q_0z)^{\frac{1}{2}}} dL dz$$

where the integration is performed in the range $10^{42} \leq L \leq 10^{47}\, erg\ s^{-1}$, according to the B94 0.3–3.5 keV XLF.

The XRB synthesis has been used to explore the evolution of the AGNs. The model was fitted to the data discussed by Gruber (1992), largely based on HEAO-1 A2 3–50 keV data[1].

Best fit parameters were determined by a χ^2-minimization procedure based on the CERN MINUIT software package.

3.1. The baseline model

The first analysis concerns the AGN1 high-redshift XLF. We tried to model the decrease of AGN1 at high redshift by introducing a new parameter $z_d \geq z_{max}$ corresponding to the onset of the space density decrease. For redshifts in the range $z_{max} < z < z_d$, the density stays constant. We used three different shapes for $z > z_d$: I) an exponential ($N(z) \propto e^{-\alpha(z-z_d)}$); II) a polinomial ($N(z) \propto (\frac{1+z}{1+z_d})^{-\alpha}$); III) a sharp cut–off ($N(z) = 0$). We allowed α to vary, and fixed z_d=4.5 (which is a simple but still good representation of the space density of AGN1 according to the present, sparse observations). For any of the laws described above, the XRB is overproduced. We then allowed also z_d to vary, always obtaining values of $z_d < 3$. This is a value much lower than observed as discussed in Sect. 2.2, and therefore all these models can be considered unacceptable.

We thus decided to adopt a sharp cut–off (model III above) with $z_d = 4.5$ and to fit the XRB changing a different parameter. We first tried to vary the number ratio R, obtaining a value of $R = 3.5 \pm 0.1$; the error corresponds to 68% confidence level, following Lampton et al. (1976). The value is still in agreement with the observations. The fit was not very satisfactory from a statistical point of view, $\tilde{\chi^2} = \frac{114.4}{41}$. Part of the high value of the $\tilde{\chi^2}$ is certainly due to the fact that we have not included other classes of sources, notably starburst galaxies and clusters of galaxies, which are likely to contribute at low energies. However, the fit is bad also at energies where we expect the AGN to dominate. The fit shows also an excess at higher energies ($E \geq 70$ keV), probably due to the value assumed for the intrinsic cut-off energy; however, as underlined in Sect. 2.1, the choice was motivated by the aim of reproducing well the $\sim$ 30–40 keV peak. Even if we know that a really good fit is impossible with any smooth model, because of the significantly large fluctuations of the data (mostly due to the fact that measurements from different instruments have been used simultaneously), we decided to try to improve the quality of the fit by further changing our baseline model.

3.2. The R(z) model

Because the evolution of type 2 AGNs is probably the least known ingredient of the model, we tried to introduce a z–dependence of the AGN2/AGN1 ratio, R. Different analytical models have been tried for $R(z)$: monotonic (both exponential and power law) shapes and King profile ($R(z) \propto \left(1 + \frac{z}{z_0}\right)^{-\alpha}$), but none of them gave a $\tilde{\chi^2}$ less than $\frac{100}{41}$.

We found, instead, a better result when a two parameter function of the form:

$$R(z) = R_0 \times (1+z)^{\alpha_1} e^{\alpha_2 z}$$

is used, with a significant improvement of the fit ($\tilde{\chi^2} = \frac{91.4}{40}$) (see Figs. 2 and 3). According to the F–test, this corresponds to a 95% confidence level with respect to the R_0=constant fit described above. The best–fit parameters are: $\alpha_1 = 1.28 \pm 0.04$, $\alpha_2 = -0.89 \pm 0.03$. The decrease of the $\tilde{\chi^2}$ is mainly due to a better reproduction of the data in the 5–10 keV energy range and around the XRB energy density peak ($\sim$30 keV).

We then checked how much dependent the above result is on the adopted shape of the local AGN spectrum, and in particular on our choice for the soft excess which, as discussed in Sect. 2.1, may be rather extreme. To do that, we adopted the opposite assumption, i.e. absence of a soft excess. The result gives an even quicker decrease of AGN2 with redshift. This is due to the fact that in absence of the soft excess the hard power law has an higher normalization in order to produce the same 0.5–

[1] Recently, a new XRB data set by the UCSD/MIT Hard X-Ray and Gamma-Ray instrument (HEAO-1 A4) has been published (Gruber et al. 1999). These data join smoothly with the XRB data reported by the GSFC HEAO-1 A2 instrument, used in this paper.

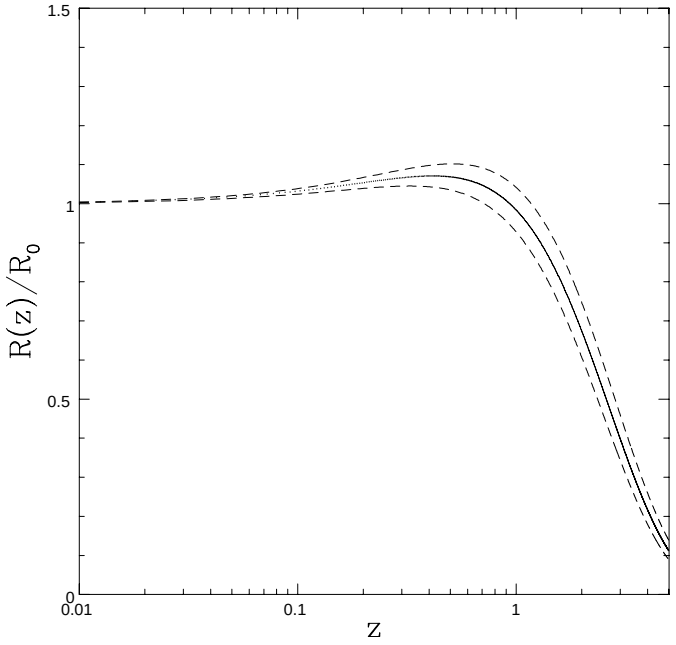

Fig. 2. The number ratio as a function of redshift $R(z)$ in unity of the local value R_0, fixing $R_0 = 4.0$ (solid line). The dashed lines enclose the 68% confidence region.

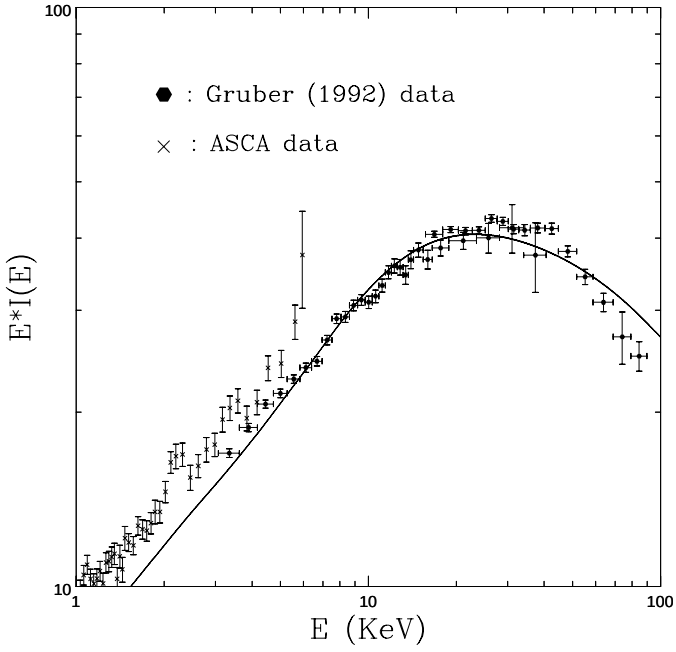

Fig. 3. The fit to the XRB data (solid line) with the $R(z)$ model; ASCA data are also reported, even though they have not been considered in the fit.

3.5 keV luminosity, which implies higher luminosity at harder energies. Thus, in order not to overproduce the XRB, less AGN2 are required.

The effect of using a pure photoelectric absorption model for AGN2, as done in some previous papers, has also been tested. In this case the spectrum intensity is higher than the photoelectric absorption + Compton scattering model (Matt et al. 1999b), and again a steeper $R(z)$ emerges.

It is important to note that the introduction of $R(z)$ implies the presence of a density evolution component for AGN2. Density evolution has been taken into account by the ROSAT All Sky Survey (RASS) 0.5–2 keV data analysis of Miyaji et al. (1998), who introduce a luminosity dependent density evolution (LDDE) basically corresponding to a sudden drop in the evolution rate at lower luminosity. However, the RASS sample contains both AGN1 and AGN2, so the authors cannot outline any differences between the two kind of sources and estimate their evolutionary properties separately.

So far we derived the AGN evolution only by fitting the XRB. Then we checked the consistency of our results with the soft (ROSAT and Einstein, 0.3–3.5 keV) and hard (BeppoSAX, 5–10 keV) counts. In Fig. 4 the source counts predicted by the model in the two bands are compared to the ROSAT (Georgantopoulos et al. 1996) + Einstein/EMSS (Gioia et al. 1990) and BeppoSAX/HELLAS (Fiore et al. 1999) data.

A good agreement in the soft band is found, while the hard counts are underestimated by a factor of ~ 1.5 at $\sim 10^{-13}$ erg cm^{-2} s^{-1}. A possible solution of this discrepancy is discussed in the next section.

3.3. The normalization

Recently, new XRB data up to 10 keV have been obtained with imaging instruments on-board ASCA (Gendreau et al. 1995, Miyaji et al. 1998) and BeppoSAX (Molendi et al. 1997, Parmar et al. 1999). While there is still some disagreement between the XRB normalizations obtained by BeppoSAX and ASCA (Parmar et al. 1999), both of them are higher than that obtained by HEAO-1. For instance, BeppoSAX/MECS result is 30% higher than the HEAO-1 (Vecchi et al. 1999).

So, we have fitted our model to the XRB introducing a 30% higher normalization to the data, but retaining the same spectral shape. According to the procedure discussed in Sect. 3.2, we first tried with a constant R_0 obtaining $R_0 = 4.9 \pm 0.1$ ($\tilde{\chi}^2 = \frac{186.7}{41}$). Again a better fit is obtained with a redshift dependence of R. The fit to $R(z)$ yields $\alpha_1 = 2.8 \pm 0.2$, $\alpha_2 = -1.5 \pm 0.1$ ($\tilde{\chi}^2 = \frac{161.9}{40}$). $R(z)$ is shown in Fig. 5, while the corresponding fit is shown in Fig. 6. With respect to the fit with the old normalization, there is a more pronounced increase of the fraction of AGN2 for z between 0.5 and 2.

The improvement is significant at the 98% confidence level, according to the F-test. It is worth noting than now ASCA data are well reproduced, even if not used in the fit. This supports the higher normalization hypothesis. Both $\tilde{\chi}^2$ are significantly higher than the fits obtained with the old normalization, mainly due to a clear deficiency of the model below $\sim$5 keV (where, however, there may be a contribution from other classes of sources). In this range the contribution of the AGN1, which cannot change in our model, is most relevant, and it was already deficient with the lower normalization. At higher energies, instead, the data are well fitted thanks to the increased number of AGN2. However, we remind that a disagreement between the

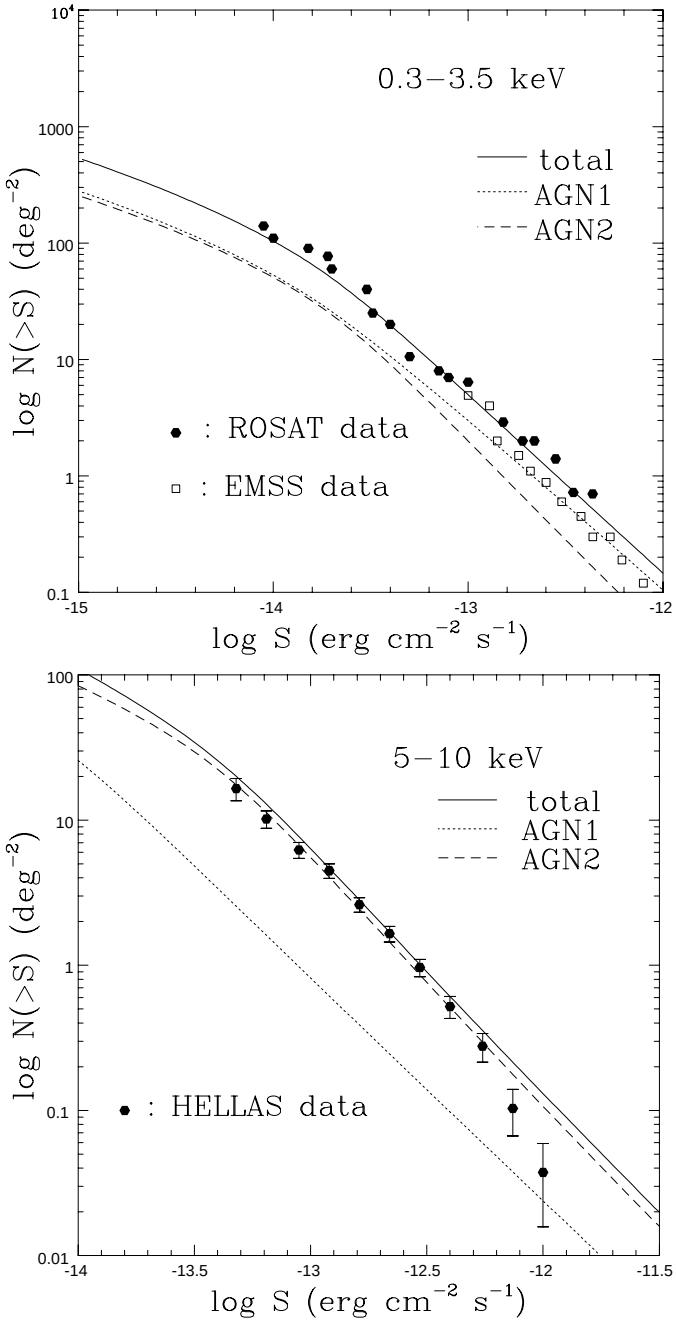

Fig. 4. (Upper panel) The integral soft counts (0.3–3.5 keV) compared to ROSAT + EMSS data. (Lower panel) The integral hard counts (5–10 keV) compared to HELLAS data. The source counts have been evaluated including the $R(z)$ term.

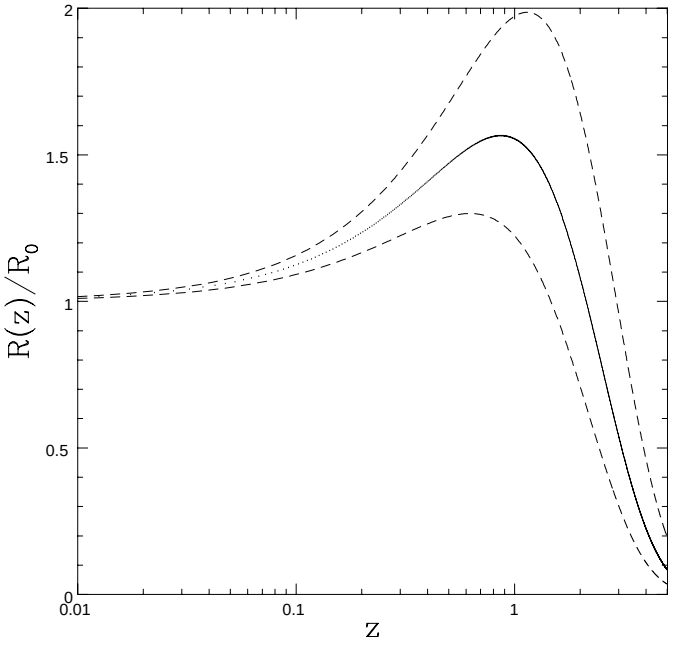

Fig. 5. Same as in Fig. 2, but introducing a 30% higher normalization to XRB data.

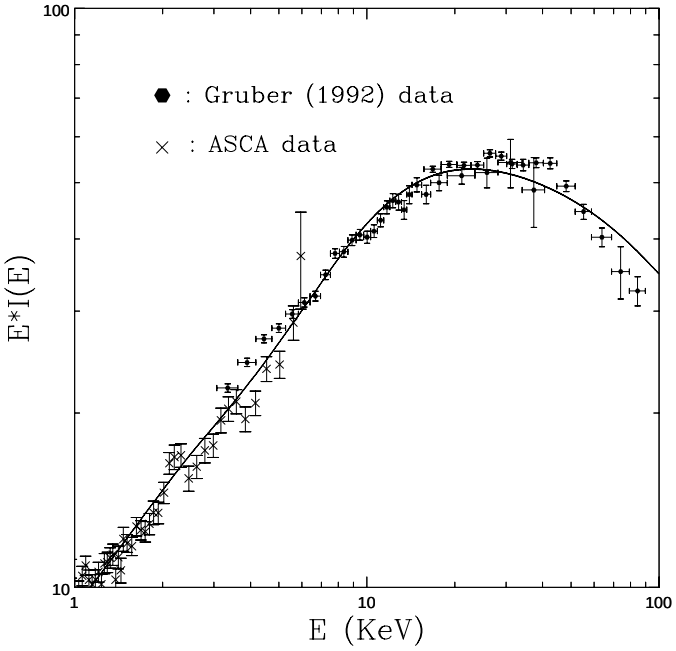

Fig. 6. Same as in Fig. 3, but introducing a 30% higher normalization to the Gruber (1992) data.

model and the data starts to emerge for $E > 70$ keV. This is unavoidable, as mentioned in Sect. 3.1, when the cut-off energy value is fixed in order to have the XRB energy density peak at ∼30–40 keV.

The most interesting result is shown in Fig. 7, illustrating soft and hard counts. The higher normalization enables to reproduce both. Even if the normalization problem must still be considered an open issue, it cannot help being noted that with the high normalization a global solution is found.

4. Discussion and conclusions

In the previous section we have discussed the possibility of a dependence on redshift of the AGN2/AGN1 ratio. In particular, this ratio remains constant or slightly increases up to $z \sim 2$, and then decreases. This would suggest that AGN2 are a later evolutionary stage of the AGN phenomenon, a possibility worth to be explored theoretically.

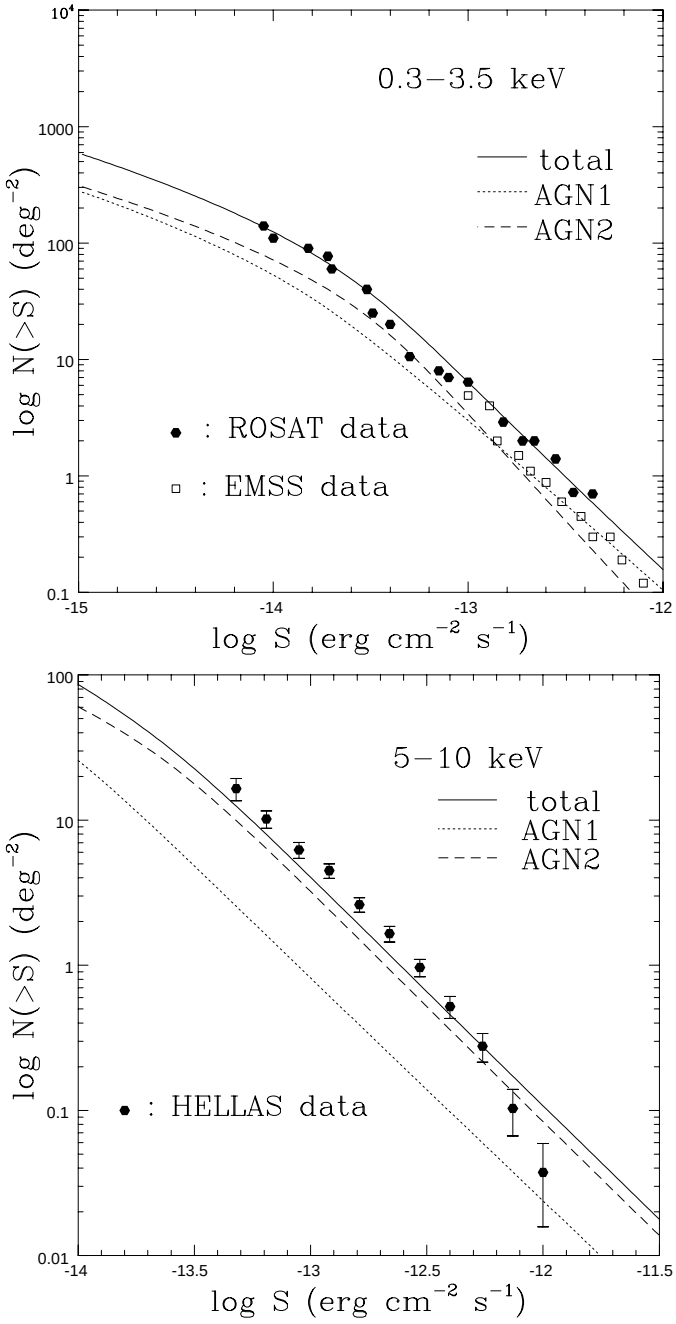

Fig. 7. Same as in Fig. 5, but introducing a 30% higher normalization to the Gruber (1992) data.

Another possibility is that the decreasing fraction of AGN2 for z $\gtrsim$ 2 is only apparent, and that in reality there is an increase of the fraction of sources with $N_H \gtrsim 10^{25}$ cm^{-2}, i.e. completely hidden at all X–ray energies. This could be linked with the star formation rate history, which is observed to increase with the redshift up to z$\sim$2, and than stays constant (Madau et al. 1996; Rowan-Robinson 1999). A high star formation rate would imply a large amount of dust and gas, and then a large absorption.

A different approach in fitting the XRB consists in a luminosity–dependent number ratio $R(L)$, as has already been done by Gilli et al. (1999b).

Table 1. AGN2 percentage prediction as a function of the sampling flux in the 5–10 keV band. The second and third column indicate the number density of AGN1 and AGN2.

Flux erg cm^{-2}s^{-1}	AGN1 deg^{-2}	AGN2 deg^{-2}	AGN2 percentage %
10^{-15}	162.8	242.1	60
5×10^{-15}	42.6	85.7	67
10^{-14}	18.3	48.3	73
5×10^{-14}	1.6	6.4	80

Table 2. Same as in Table 1, but introducing a 30% higher normalization to the Gruber (1992) data.

Flux erg cm^{-2}s^{-1}	AGN1 deg^{-2}	AGN2 deg^{-2}	AGN2 percentage %
10^{-15}	162.8	299.3	65
5×10^{-15}	42.6	115.2	73
10^{-14}	18.3	69.2	79
5×10^{-14}	1.6	11.3	88

The direct way to discriminate between different evolutionary models is to study the AGN2 XLF, a task within the capabilities of the new generation X–ray missions (*Chandra* and XMM).

In Table 1 and Table 2 we report the AGN1 and AGN2 densities for different flux limits corresponding to the $R(z)$ models without and with the inclusion of the 30% increase in the normalization of the XRB. The effect of $R(z)$ shows up in an AGN2 percentage decreasing at lower fluxes, a consequence of the sampling at higher redshifts where the AGN2/AGN1 number ratio decreases. It is worth noting that 10^{-15} erg cm^{-2} s^{-1} and 5×10^{-15} erg cm^{-2} s^{-1} are the flux limits expected for the Deep observations of the Lockman Hole and the Hubble Deep Field scheduled for *Chandra* and XMM, respectively.

Acknowledgements. We wish to thank the BeppoSAX Scientific Data Center for assistance and the HELLAS group for the useful and stimulating collaboration. We would also like to thank F.Fiore, P.Giommi, A.Comastri, S.Molendi and A.Vecchi for supplying us the data involved in this work and for several useful discussions, R.Gilli, G.Risaliti and M.Salvati for valuable comments on the manuscript and the referee Dr.W.Brinkmann for suggestions to improve the final version. This work was partially supported by the Italian Space Agency, and by the Ministry for University and Research (MURST) under grant COFIN98–02–3

References

Antonucci R.R.J., Miller J.S., 1985, ApJ 297, 621
Boyle J., Shanks T., Georgantopoulos I.G., Stewart G.C., Griffiths R.E., 1994, MNRAS 271, 639
Boyle J., Wilkes B.J., Elvis M., 1997, MNRAS 285, 511
Celotti A., Fabian A.C., Ghisellini G., Madau P., 1995, MNRAS 277, 1169
Comastri A., Setti G., Zamorani G., Hasinger G., 1995, A&A 296, 1
Comastri A., Fiore F., Giommi P., et al., 1999, Adv. Space Rev., in press, astro-ph/9902060

Fiore F., Giommi P., La Franca F., et al., 1999, In: Proceedings of X-ray Astronomy. Stellar Endpoints, AGN and the Diffuse X-ray Background, in press
Gendreau K.J., Mushotzky R., Fabian A.C., et al., 1995, PASJ 47, L5
Georgantopoulos I.G., Stewart G.C., Shanks T., Boyle J., Griffiths R.E., 1996, MNRAS 280, 276
Gilli R., Comastri A., Brunetti G., Setti G., 1999a, New Astron. 4, 45
Gilli R., Risaliti G., Salvati M., 1999b, A&A in press, astro-ph/9904422
Gioia I., Maccacaro T., Schild R.E., et al., 1990, ApJS 72, 567
Goodrich R.W., Veilleux S., Hill G.J., 1994, ApJ 422, 521
Gruber D.E., 1992, In: Proceedings of Extragalactic Background Radiation: a meeting in honor of Riccardo Giacconi. Cambridge University Press
Gruber D.E., Matteson J.L., Peterson L.E., Jung G.V., 1999, in press, astro-ph/9903492
Hasinger G., 1998, Astron. Nachr. 319, 1
Ho L.C., Filippenko A.V., Sargent W.L.W., 1997, ApJ 487, 568
Huchra J., Burg R., 1992, ApJ 393, 90
Jones L.R., McHardy I.M., Merrifield M.R., et al., 1997, MNRAS 285, 547
Kennefick J.D., Djorgovsky S.G., Meylan G., 1996, AJ 111, 1816
Lampton M., Margon B., Bowyer S., 1976, ApJ 208, 177
Madau P., Ghisellini G., Fabian A.C., 1994, MNRAS 270, L17
Madau P., Ferguson H.C., Dickinson M.E., et al., 1996, MNRAS 283, 1388
Magdziarz P., Zdziarski A., 1995, MNRAS 273, 837
Maiolino R., Rieke G.H., 1995, ApJ 454, 95
Maiolino R., Salvati M., Bassani L., et al., 1998, A&A 338, 781
Marshall F.L., Boldt E.A., Holt S.S., et al., 1980, ApJ 235, 4
Matsuoka M., Piro L., Yamauchi M., Murakami T., 1990, ApJ 361, 440
Matt G., Fabian A.C., 1994, MNRAS 267, 187
Matt G., Guainazzi M., Maiolino R., et al., 1999a, A&A 341, L39
Matt G., Pompilio F., La Franca F., 1999b, New Astron. 4, 191
Miyaji T., Hasinger G., Schmidt M., 1998, In: Highlights in X-ray Astronomy in Honor of Joachim Treumper's 65th birthday. MPE Report, MPE, Garching, in press, astro-ph/989398
Molendi S., Chiappetti L., Cusumano G., et al., 1997, Mem. Soc. Astron. Ital. 68, n.1/2, 113
Morrison R., McCammon D., 1983, ApJ 270, 119
Nandra K., Pounds K.A., 1994, MNRAS 268, 405
Page M.J., Carrera F.J., Hasinger G., et al., 1996, MNRAS 281, 579
Parmar A.N., Guainazzi M., Osterbroek T., et al., 1999, A&A 345, 611
Pounds K.A., Nandra K., Stewart G.C., George I.M., Fabian A.C., 1990, Nat 344, 132
Risaliti G., Maiolino R., Salvati M., 1999, ApJ, in press, astro-ph/9902377
Rowan-Robinson M., 1999, In: Lutz D., Tacconi L. (eds.) Proceedings of the Ringberg Workshop on Ultra-Luminous Galaxies: Monsters or Babies? in press on Astrophys. Space Sci., astro-ph/9906308
Schwartz D.A., 1992, In: Barcons X., Fabian A.C. (eds.) The X-Ray Background. Cambridge University Press
Setti G., Woltjer L., 1989, A&A 224, L21
Shaver P.A., Hook I.M., Jackson C.A., et al., 1999, to appear in: Carilli C., Radford S., Menten K., Langston G. (eds.) Highly Redshifted Radio Lines. in press
Vecchi A., Molendi S., Guainazzi M., et al., 1999, A&A 349, L73
Wilman R.J., Fabian A.C., 1999, MNRAS, in press, astro-ph/9907204